**Detection and Tracking of Astral Microtubules in Fluorescence Microscopy Images**

# DETECTION AND TRACKING OF ASTRAL MICROTUBULES IN FLUORESCENCE MICROSCOPY IMAGES

*Joshua Levine, Marco Grangetto*

Università degli Studi di Torino
Computer Science dept.
Corso Svizzera 185, Torino, Italy

*Marilena Varrecchia, Gabriella Olmo*

Dept. of Control and Computing Engineering
Politecnico di Torino
Corso Duca degli Abruzzi 24, Torino, Italy

## ABSTRACT

In this paper we explore detection and tracking of astral microtubules, a sub-population of microtubules which only exists during and immediately before mitosis and aids in the spindle orientation by connecting it to the cell cortex. Its analysis can be useful to determine the presence of certain diseases, such as brain pathologies and cancer. The proposed algorithm focuses on overcoming the problems regarding fluorescence microscopy images and microtubule behaviour by using various image processing techniques and is then compared with three existing algorithms, tested on consistent sets of images.

***Index Terms*—** Medical diagnostic imaging, fluorescence microscopy, image segmentation, kalman filter, microtubules

## 1. INTRODUCTION

Microtubules are a type of protein polymer that make up the cellular *cytoskeleton*, an array of filaments that are used to establish cell shape and assist with cell division, by forming a structure called the *mitotic spindle*, which segregates the chromosomes into the two daughter cells.

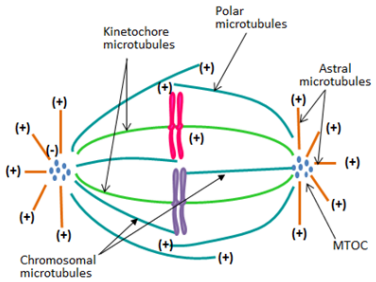


Microtubule behaviour can be described as two alternating states: *polymerization* (growth) and *depolymerization* (shrinkage). In a population of microtubules, a subset of microtubules is rapidly growing while others are quickly shrinking (although sometimes they are in a paused state) and individual microtubules randomly switch between the two states [1], thus complicating the process of tracking them. This property is often called *dynamic instability* [1].

For this project, we are considering microtubules in doped cells, in order to have better knowledge regarding their behaviour. The used drugs are *taxol* and *nocodazole*. At high concentration, both agents have a similar effect on the mitosis process and, by increasing the dosage, it is possible to inhibit the growth of microtubules, thus making their behaviour more predictable.

Microtubules are analyzed via fluorescence microscopy, thanks to fluorofores that selectively bind the plus-end of these polymers. Fluorescence microscopy images have two main issues: the presence of *shot noise*, which cannot be reduced with standard additive noise-removal techniques, as it depends on the signal itself, and the dynamic instability of microtubule behaviour, which makes tracking very challenging. Nowadays, detection and tracking of microtubules is still, for the most part, manually done, which is a tedious and time-consuming process. Thus, in the last few years, a lot of attention was put in developing algorithms that could automatically carry out this task.

## 2. BACKGROUND

One of the main issues of the goal we pursued is represented by the resolution of the microscopes: even the best performing microscopes have a resolution of about 100 nm [2], which is greater than the typical size of microtubules (25 nm [1]). Thus, it is hard to determine whether an element is a structure of interest or just part of the background.

Another major issue is the presence of *shot noise*, which entails a very low SNR (*Signal-to-Noise Ratio*). This problem is present when the images are *in vivo* and the lighting intensity is reduced to a minimum value to prevent the damaging of the cells and *photobleaching*, which is the photochemical alteration of a dye or a fluorophore molecule such that it permanently is unable to fluoresce. For this project, the adopted measure to evaluate the SNR is the PSNR (Peak Signal-to-Noise Ratio) defined as $PSNR = 10\log_{10}\frac{P^2}{MSE}$, where $P$ is the maximum intensity value of the pixels (peak) and $MSE$ is the mean squared error between the considered images and an image containing only noise. Determining the latter is not a trivial task and there is no automatic way to achieve it. In this case, the images were analyzed and a region that was assumed containing only noise was used for this purpose.

## 3. THE PROPOSED TECHNIQUE

The algorithm is divided into three main steps: enhancement, detection and tracking.

The **enhancement** process focuses on reducing the amount of noise affecting the image. Microscope images are affected by classic shot noise with Poisson distribution caused by photon counting. The method we adopt to reduce shot noise is based on the classic

The authors thank Prof. Di Cunto, and Doct. Gai of Department of Molecular Biotechnology and Health Sciences, University of Torino for having provided the image data.

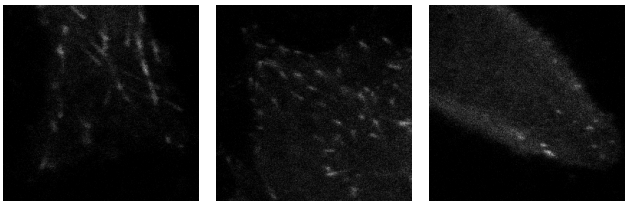

**Fig. 1**: Fluorescence microscopy images of microtubules. The plus ends of the latter are highlighted by the fluorophores during the polymerization phase.

*Anscombe transform* [3] pre-processing, which turns random variables with a Poisson distribution into a Gaussian distribution with an approximately constant standard deviation. This amounts at mapping each input image $f$ onto the transformed image $g$ according to:

$$f \rightarrow g = 2\sqrt{f + \frac{3}{8}} \tag{1}$$

Then denoising is applied in the Anscombe domain using *Wiener* filtering [4], getting $\hat{g} = h_w * g$, where $h_w$ denotes the impulse response of the filter and operator $*$ represents the convolution. As a further enhancement step, we apply a Difference of Gaussians (DOG) filter [4]. The standard deviations of the filter pair, denoted as $\sigma_1$ and $\sigma_2$, need to be tuned according to the image Signal-to-Noise Ratio (see experimental section for details). Finally, the denoised image is obtained by applying the *inverse Anscombe* transformation given by

$$\hat{f} \rightarrow \left(\frac{\hat{g}}{2}\right)^2 - \frac{3}{8} \tag{2}$$

In Fig. 2b the effect of the enhancement stage is visually shown.

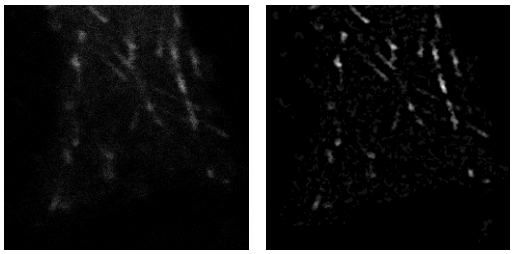

(a) (b)

**Fig. 2**: Example of original image (a) and enhanced image (b).

The **detection** phase focuses on locating microtubules and identifying the peak (local maxima) in each region corresponding to one microtubule plus-end. The peak is the pixel that will be used for the following tracking phase. In this stage we relied on both gray-scale and binary *morphological transformations* to limit the effect of noise on the following segmentation.

The *gray-scale erosion* operator defined as

$$\hat{f}_e = (\hat{f} \ominus b)(s,t) = min\{\hat{f}(s+x, t+y) - b(x,y) | \\ (s+x), (t+y) \in D_f; (x,y) \in D_b\}$$

is applied to image $\hat{f}$ in order to reduce noise and even out the background. The structuring element $b$ is defined as a $3 \times 3$ window, which is invariant with respect to the $x$ and $y$ axes, as no assumption can be made regarding the orientation of the microtubules. Then, a binary image is computed as $m = \hat{f}_e > 0$, i.e. every pixel with an intensity greater than 0 is set to 1. Finally, the binary mask $m$ is refined with an *area opening* morphological operation followed by *dilation*: the first step in order to remove spurious components that are smaller than a predefined area, the second to avoid having single microtubules segmented into different pieces.

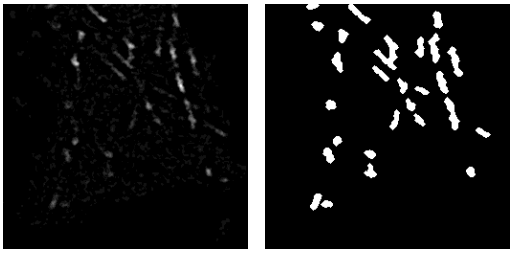

(a) (b)

**Fig. 3**: Enhanced image (a) and corresponding binary mask $m$ (b).

The last step of the detection phase is to define the local intensity maxima in order to identify the microtubules with a single pixel at a given location. This is done by masking the enhanced image $\hat{f}_e$ with the binary mask $m$ obtained above. The masked image will ideally contain only the regions representing microtubules, which are used to calculate the local maxima. In order to get smoother regions that simplify the computation of the local maxima, the masked image is further blurred with a Gaussian filter with parameter $\sigma_3$. Finally, to identify the peaks, a $5 \times 5$ window is used: the local maxima are defined as those pixels that, compared to their 24 neighboring pixels, have the highest intensity. Fig. 4 visually summarizes the process we described showing the original image (a), the segmentation mask $m$ (b) and the location of microtubules peaks (c), respectively.

(a) (b) (c)

**Fig. 4**: Original image (a), segmentation binary mask $m$ (b) and masked image with microtubules peaks highlighted in red.

**Tracking** is the final step and it allows to retrieve information regarding velocity, length and number of microtubules from a given stack. Once the microtubules are detected in every image, it is necessary to define their trajectory. The tracking process is achieved by using the Kalman filter.

Tracking is based on the assumption that microtubules exhibit a uniform rectilinear motion [1]. Let us denote as $\vec{X}_t = (x_{t,1}, x_{t,2}, \ldots, x_{t,N})$ and $\vec{Y}_t = (y_{t,1}, y_{t,2}, \ldots, y_{t,N})$ the pixel coordinates of the $N$ microtubules peaks identified in the $t$-th frame of the image stack. The coordinates $\langle \vec{X}_t, \vec{Y}_t \rangle$ define the state for a certain frame $t$ and are used, along with the dynamic model, i.e. rectilinear uniform motion, to predict the positions $\langle \hat{X}_{t+1}, \hat{Y}_{t+1} \rangle$ of

the microtubules in the subsequent frame $t+1$. Such predictions are compared with the detected peaks' coordinates in frame $t+1$ and possibly put into a one-to-one correspondence.

$$\langle \vec{X}_t, \vec{Y}_t \rangle \xrightarrow{\text{prediction}} \langle \hat{X}_{t+1}, \hat{Y}_{t+1} \rangle \xleftarrow{\text{assignment}} \langle \vec{X}_{t+1}, \vec{Y}_{t+1} \rangle \quad (3)$$

The assignment is based on the Euclidean distances between the detected peaks and the predictions; the *Hungarian method* [5] has been used in order minimize the distances between every pair. In turn, the assignments allow one determine the path followed by a given microtubule (let us say the $k$-th one) that we denote as a track $T^k = \langle \vec{X}^k, \vec{Y}^k \rangle$, where $\vec{X}^k = (x_{1,k}, x_{2,k}, \ldots, x_{t,k})$ and $\vec{Y}^k = (y_{1,k}, y_{2,k}, \ldots, y_{t,k})$ represent the temporal sequence of peak coordinates occupied by the given microtubule. The low SNR of the processed images makes the assignment phase in (3) very critical. Usually, assignments characterized by an Euclidean distance between prediction and actual detection larger than a given threshold, are considered to be unlikely and discarded. In this work we propose a simple, yet effective, strategy for the computation of the threshold; moreover, the threshold is adjusted adaptively, taking into account the dynamics of each track. To this end, for each track, we define the temporal disparity at time $t$ as

$$d_t^k = \sqrt{(x_{t,k} - x_{t-1,k})^2 + (y_{t,k} - y_{t-1,k})^2}$$

At time $t$ the dynamic behavior of $T^k$ is characterized by the average disparity and corresponding standard deviation, estimated by

$$\bar{d}_t^k = \frac{\sum_{i=1}^{t-1} d_i^k}{t-1} \qquad (4)$$

$$\sigma_t^k = \sqrt{\frac{\sum_{i=1}^{t-1} (d_i^k - \bar{d}_t^k)^2}{t-2}}$$

Finally, assignment of $k$-th track in frame $t$ is accepted only if the distance between prediction and detection is lower than threshold $\tau^k = \bar{d}_t^k + \sigma_t^k$.

After the assignment step, the detected peaks that do not correspond to any previous path are used to start new tracks in frame $t$. At the same time, previous tracks estimates that cannot be matched in frame $t$ are flagged by increasing a penalty score $S^k$; the estimated coordinates $\langle \hat{x}_{t,k}, \hat{y}_{t,k} \rangle$ are temporarily considered as the new position of the microtubule for future tracking attempts. If a new assignment is found for track $k$ with $S^k \leq \Delta$ then track $T^k$ is considered as an active one (flag is reset as $S^k = 0$), in the opposite case it is ended. This allows us to consider as single tracks microtubules that momentarily disappear due to depolymerization (i.e. depolymerization does not activate the fluorophore). In Fig. 5 an example of the evolution of the tracked microtubules (red dots) in 3 frames with $t = 1, 10, 20$ is shown.

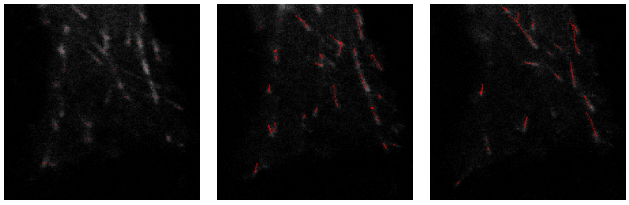

**Fig. 5**: Evolution of tracked microtubules (red dots) in 3 frames with $t = 1, 10, 20$ from left to right.

After all frames in the stack have been processed one gets a list of microtubule tracks, whose behaviour can be analyzed. In particular, in this work we consider the space covered by each microtubule, usually termed as length, and the corresponding velocity.

## 4. PERFORMANCE EVALUATION

Our results are based upon fluorescence microscopy image stacks made available by the Department of Molecular Biotechnology and Health Sciences, University of Torino. A HeLa Kyoto cell line, expressing the fluorescent protein EB3-td Tomato, was chosen to carry out the experiments [6]. The cell culture was maintained in DMEM-GlutaMAX (Invitrogen) medium supplemented with 10% fetal bovine serum, 100 U ml$^{-1}$ penicillin, 100 $\mu$g ml$^{-1}$ streptomycin, 200 $\mu$g ml$^{-1}$ geneticin (Sigma) and 0.5 $\mu$g ml$^{-1}$ puromycin. Interphase cells were treated with increasing concentrations of nocodazole and taxol: 0 nM (control), 10 nM and 100 nM. Even though their actions on microtubule dynamics are different and to some extent not completely explained, the neat effect of these drugs, at high concentrations, is an inhibition of dynamic instability. After 1 hour incubation, videos of astral microtubules were acquired using a Leica TCS SP5-AOBS 5-channel confocal system, equipped with a 561 nm DPSS laser. During the acquisition, cells were stored in the microscope incubator at 37 °C with $CO_2$ 5%. The main characteristics of the image stacks are summarized in Table 1.

| Description | Value |
|---|---|
| Frame size | $256 \times 256$ pixels |
| Frame rate | 2 fps |
| Number of frames per stack | 120 |
| Pixel resolution | 64 nm |
| Bit depth | 8 |

**Table 1**: Main characteristics of employed images.

To evaluate the proposed algorithm, five stacks have been considered for each concentration of nocodazole and taxol. Results have been worked out in terms of track velocity and length, and number of detected microtubules. The results obviously depend on the chosen parameters for the algorithm, which are displayed in Table 2.

| Parameters | Description | Value |
|---|---|---|
| $\sigma_1$ | First Gaussian kernel (DOG) | 1 |
| $\sigma_2$ | Second Gaussian kernel (DOG) | 3-4 (*) |
| $\sigma_3$ | Gaussian kernel (local maxima) | 1 |
| $\Delta$ | Allowed penalties (Kalman) | 3 |

(*) $\sigma_2 = 3$ if $PSNR < 24.5$ dB; $\sigma_2 = 4$ if $PSNR \geq 24.5$ dB.

**Table 2**: Algorithm parameters.

The obtained results have been compared with those yielded by two existing algorithms: *Applegate* [7] and *Sironi* [8]. However, it is worth pointing out that these algorithms have been tested on different data, not made available by the authors. A further approach, being developed at the Politecnico of Torino (*Polito*) [6], is being tested on the same stacks. The algorithm [6] does not use morphological operators to reduce false positive detections but it comprises a calibration phase. Preliminary comparison results are included in this paper.

### 4.1. Nocodazole results

Table 3 reports the mean value $\mu$ and the standard deviation $\sigma$ of microtubule velocity and length, as well as the number of detected tracks, evaluated on cell cultures doped with nocodazole.

| NOCODAZOLE | | | | | |
|---|---|---|---|---|---|
| Conc. | $\mu$ Vel. | $\sigma$ Vel. | $\mu$ Len. | $\sigma$ Len. | MT number |
| 0 | 16.23 | 13.43 | 1.00 | 1.41 | 393.8 |
| 10 | 19.92 | 15.53 | 1.12 | 1.49 | 461.6 |
| 100 | 11.20 | 10.51 | 0.34 | 0.40 | 180.0 |

**Table 3**: Nocodazole results

First of all, it can be appreciated that at concentration 100 nM, all values are significantly lowered. This is coherent with the well known fact that high-concentration nocodazole inhibits polymerization. On the other hand, at concentration 10 nM, average velocity and track length turn out to be increased with respect to controls. This can be explained noticing that, at low concentrations, nocodazole inhibits microtubule dynamic instability [9], thus favouring the growth of polymerizing microtubules and the shrinkage of depolymerizing ones. As microtubule plus-ends are visible only during the polymerization phase, higher velocities and lengths are observed. It is worth pointing out that this result, although theoretically sound, has been seldom verified in actual experiments.

As for the number of detected microtubules, it turns out to be quite high, especially if compared with those which can be manually tracked. This is due to specific parameter choices, and implies that also very short tracks, which cannot be manually appreciated, are taken into account by the algorithm. This can possibly yield lower average track lengths, but we have verified that it has little impact on the average track velocity.

### 4.2. Taxol results

Table 4 displays the results regarding taxol effects on microtubule dynamic behaviour. Taxol is known to inhibit polymerization in a way that is directly dependent on its concentration [10]. Our results are coherent with this consideration, as they show a monotonically decreasing behaviour of both track velocity and length, with the largest gap between 0 nM and 10 nM.

| TAXOL | | | | | |
|---|---|---|---|---|---|
| Conc. | $\mu$ Vel. | $\sigma$ Vel. | $\mu$ Len. | $\sigma$ Len. | MT number |
| 0 | 22.67 | 17.92 | 1.20 | 1.70 | 428.0 |
| 10 | 11.06 | 9.34 | 0.45 | 0.55 | 177.0 |
| 100 | 8.66 | 8.86 | 0.29 | 0.34 | 38.4 |

**Table 4**: Taxol results

### 4.3. Comparison

Fig. 6 reports comparisons among our algorithms and other similar methods already published in literature, in terms of average velocity and length as functions of different drug concentrations.

From figure 6, it is clear that the algorithms labelled *Applegate* and *Sironi* return different values for both velocities and lengths, as they were tested on different stacks. Thus, the only meaningful comparison is on trends and orders of magnitude of the quantities involved. As a general consideration, we can appreciate that the algorithms yield the same order of magnitude of both velocity and length. However, our algorithm, with respect to *Applegate* and *Sironi*, is able to put into evidence the non monotonic behaviour of velocity as a function of nocodazole concentration. As already discussed, this result confirms a feature of this drug that was theoretically hypothesized but seldom verified in practice.

As for the comparisons with the algorithm labelled *Polito*, we can notice that the trends yielded by the two algorithms are comparable. Both of them put into evidence the typical behaviour of nocodazole-doped cells. In the case of taxol-doped cultures, the trend of track velocity is similar, with our algorithm yielding slightly lower values. As for lengths, it is worth noticing that our algorithm provides lower values especially at high drug concentrations. Actually, the *Polito* algorithm makes a different choice in the track selection stage. In fact, tracks whose length is below 5 frames are discared, as they are assumed not to match the uniform rectilinear motion assumption. Clearly, this slightly polarizes the results in term of a lower average length provided by our algorithm.

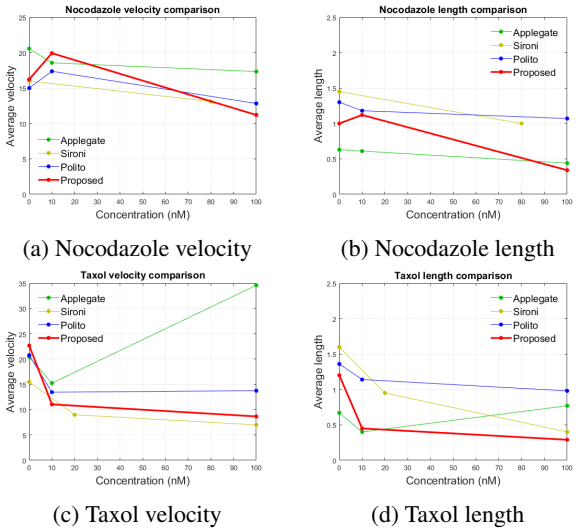


(a) Nocodazole velocity (b) Nocodazole length

(c) Taxol velocity (d) Taxol length

**Fig. 6**: Results for nocodazole (figures 6a and 6b) and taxol (figures 6c and 6d) given by the different algorithms. In *red* are highlighted the results of the proposed algorithm.

## 5. CONCLUSIONS AND FUTURE WORKS

The proposed algorithm is able to efficiently detect and track microtubules in fluorescence microscopy images, by adopting various image processing techniques. Our method focuses on limiting false positives in order to have accurate results. The obtained results are promising if compared with the expected microtubule behaviour at increasing concentrations of both nocodazole and taxol. Moreover, by analyzing the sequence of images displaying the tracks, it is clear that the algorithm successfully detects microtubules without capturing false positives, given by noise affecting the images.

Future works include defining a more robust way to compute the SNR, which is used to define the $\sigma$ values of the difference of Gaussians, which, at the moment, depend on the single stacks; implement the algorithm as an *ImageJ* plug-in in order to provide a user-friendly interface and an out-of-the-box usable application.

## 6. REFERENCES


[1] Kendra S. Burbank and Timothy J. Mitchison, "Microtubule dynamic instability," *Current Biology*, vol. 16, no. 14, pp. R516 – R517, 2006.

[2] I. Smal, M. Loog, W. Niessen, and E. Meijering, "Quantitative comparison of spot detection methods in fluorescence microscopy," *IEEE Transactions on Medical Imaging*, vol. 29, no. 2, pp. 282–301, Feb 2010.

[3] F. J. Anscombe, "The transformation of poisson, binomial and negative-binomial data," *Biometrika*, vol. 35, no. 3/4, pp. 246–254, 1948.

[4] Rafael C. Gonzalez and Richard E. Woods, *Digital Image Processing (3rd Edition)*, Prentice-Hall, Inc., Upper Saddle River, NJ, USA, 2006.

[5] B. Sahbani and W. Adiprawita, "Kalman filter and iterative-hungarian algorithm implementation for low complexity point tracking as part of fast multiple object tracking system," in *2016 6th International Conference on System Engineering and Technology (ICSET)*, Oct 2016, pp. 109–115.

[6] Varrecchia M., Olmo G., Levine J., Grangetto M., Gai M., and Di Cunto F., "Automatic microtubule tracking in fluorescence images of cells doped with increasing concentrations of taxol and nocodazole," *preprint available at https://arxiv.org/abs/1802.01553*, 2018.

[7] Kathryn T. Applegate, Sebastien Besson, Alexandre Matov, Maria H. Bagonis, Khuloud Jaqaman, and Gaudenz Danuser, "plustiptracker: Quantitative image analysis software for the measurement of microtubule dynamics," *Journal of Structural Biology*, vol. 176, no. 2, pp. 168 – 184, 2011.

[8] Lucia Sironi, Jérôme Solon, Christian Conrad, Thomas U Mayer, Damian Brunner, and Jan Ellenberg, "Automatic quantification of microtubule dynamics enables rnai-screening of new mitotic spindle regulators," *Cytoskeleton*, vol. 68, no. 5, pp. 266–278, 2011.

[9] Keliang Xu, Patricia M Schwarz, and Richard F Ludueña, "Interaction of nocodazole with tubulin isotypes," *Drug development research*, vol. 55, no. 2, pp. 91–96, 2002.

[10] Anne-Marie C Yvon, Patricia Wadsworth, and Mary Ann Jordan, "Taxol suppresses dynamics of individual microtubules in living human tumor cells," *Molecular biology of the cell*, vol. 10, no. 4, pp. 947–959, 1999.